nature communications

Article

https://doi.org/10.1038/s41467-025-65310-0

Twisted-stacking MOF patterns with tailorable circularly polarized luminescence properties and encryption applications

Received: 5 June 2025

Accepted: 7 October 2025

Published online: 24 November 2025

Check for updates

Xini Chu[1,4], Jingguo Li[2,4], Di Wang[1], Liyu Gan[1], Xu Liu[1], Zeyu Feng[1], Peng Yang[1], Hongli Zhang[1] ✉, Yifan Xie[1] ✉, Fei Wang[3] ✉ & Gang Zou[1] ✉

Optical active metal-organic frameworks (MOFs) with circularly polarized luminescence (CPL) functionalities, have recently gained extensive research interest. However, the luminescence dissymmetry factors (g_{lum}) of these materials are generally small, and the lack of patterning ability for most optical active MOFs greatly hinders their practical applications. Herein, we report a strategy to design twisted-stacking MOF patterns with a high g_{lum} (~0.4) and tailorable CPL performance by the combination of brush coating, bottom-up heteroepitaxial growth and twisted-stacking techniques. Specifically, two-dimensional (2D) programmable patterns of highly oriented MOF films could be achieved by the heteroepitaxial growth from pre-aligned $Cu(OH)_2$ nanowire (NW) templates. The oriented MOF patterns could be functionalized with fluorescent dyes, offering characteristic anisotropic photoluminescent response. After another similar highly oriented MOF layer was deposited on top of the above MOF/dye patterns (in a twisted fashion) as a phase retarder, a chiroptical response could be generated. This design not only allows the fabrication of arbitrary programmable optical active MOF patterns with enhanced g_{lum}, but also enables precise regulation of CPL performance within the patterns, favoring the implementation of the miniaturized chiroptical devices, information encryption and storage.

Metal-organic frameworks (MOFs), assembled through metal ions or clusters and organic struts[1,2], have attracted enormous attention owing to their structural regularity, well-defined pore size, and variable chemical functionality[3–7], and are playing an important role in host-guest chemistry for a wide range of applications such as catalysis, gas storage, chemical sensing, and so on[8–11]. Among them, optical active MOFs with chiral structure and function have aroused great interest in enantioselective separation, asymmetric catalysis, and chiroptical applications[12–14]. In particular, the integration of chirality transfer and luminescence properties in MOFs is a strategy for endowing and further amplifying their circular polarized luminescence (CPL) performance[15]. Many strategies have been explored to construct optical active MOFs, primarily involving direct methods using chiral linkers or co-linkers, post-modification, spontaneous resolution, and chiral induction[16,17]. However, in most cases, the luminescence dissymmetry factors (g_{lum}) of these materials are very small, ranging from 10^{-3} to 10^{-2}, limiting their practical applications. Significant efforts have been made to further enhance the g_{lum} values of optical active MOFs

[1]State Key Laboratory of Precision and Intelligent Chemistry, School of Chemistry and Materials Science, University of Science and Technology of China, Hefei, Anhui, China. [2]State Key Laboratory of Advanced Environmental Technology, Department of Environmental Science and Engineering, University of Science and Technology of China, Hefei, Anhui, China. [3]Division of Life Sciences and Medicine, The Department of Neurosurgery, The First Affiliated Hospital of USTC, University of Science and Technology of China, Hefei, Anhui, China. [4]These authors contributed equally: Xini Chu, Jingguo Li.
✉e-mail: zhl1992@ustc.edu.cn; yfxie@ustc.edu.cn; neurosurgeonwf1@ustc.edu.cn; gangzou@ustc.edu.cn

materials[18–22]. Gu et al. reported a chiral liquid crystalline MOF to realize highly CPL performance with photo and thermal switching[23]. Duan and colleagues developed an up-conversion and downshifting CPL in chiral MOFs with a high g_{lum} value up to 0.1 based on the specific host-guest interactions[24]. Despite numerous advances in CPL-switchable MOFs research, there is a long-standing quest to find a generic strategy to develop CPL MOFs materials with both high g_{lum} and localized dynamic switching function (including CPL magnitude and wavelength) so that the demands of practical applications can be met. Compared with the well-established technique using chiral ligands or dopants, twisted-stacking of multiple achiral anisotropic functional layers is receiving increasing attention for fabricating chiroptical films with high g_{lum} value[25–28]. Tang et al. reported the fabrication of biomimetic chiral photonic crystals with a g_{lum} of 0.8[29]. Kuang and colleagues developed the twisted-stacking of CdSe@CdS nanorod assemblies with a notable g_{lum} of 0.2[30]. It is expected that combining advances in twisted-stacking techniques with stimuli-responsive fluorescent (FL) MOFs will yield innovative optical active MOFs with enhanced g_{lum} and switchable CPL performance. However, the fabrication of programmable optical active MOFs with both high g_{lum} and multi-responsive functionalities based on twisted-stacking strategy has not been reported.

Patterning optical active MOF components in situ at the microscale with tailorable CPL performance is highly desirable, as it is crucial for the integration of optical active MOFs into microdevices, promoting their applications in chiral optoelectronics and information encryption technologies. Traditional lithographic techniques such as photolithography could produce micro- or nano-sized patterns of MOFs[31–35]. However, only a few studies describe the fabrication of aligned MOF patterns with anisotropic properties. Ameloot and colleagues developed a strategy that combined bottom-up self-assembly of an oriented MOF film and top-down lithography to enable the fabrication of MOF patterns with oriented crystal structure[35]. Falcaro et al. reported the fabrication of oriented MOF patterns using a resist-free protocol and obtained anisotropic photoluminescent responses by incorporating fluorescent dyes within the aligned MOFs channels[36]. Up to date, it remains a great challenge for in situ patterning of optical active MOFs with enhanced g_{lum} and tailorable CPL performance in a feasible and economical fashion.

Herein, we demonstrate experimentally that the fabrication of 2D programmable MOF patterns with highly oriented crystalline structures by combining the brush coating technique and the bottom-up heteroepitaxial growth strategy. The fabrication of arbitrary programmable oriented $Cu(OH)_2$ patterns could be achieved via a brush coating process, where highly aligned $Cu(OH)_2$ nanowires acted as a sacrificial template to induce the heteroepitaxial growth of oriented crystalline MOF films. Upon incorporation of fluorescent dyes, the resultant oriented MOF patterns exhibited programmable anisotropic photoluminescent response. Employing similar step-wise brush coating and heteroepitaxial growth processes, another highly oriented MOF layer could be fixed on top of the bottom MOF/dye patterns in a twisted fashion, which act as a phase retarder to generate CPL response based on a Jones Matrix mechanism (Fig. 1a). The wavelength, magnitude and handedness direction of CPL performance of the designed patterns could be precisely controlled, more importantly, the gradient distribution of CPL intensity and arbitrary programmable CPL patterns could be easily achieved, favoring their potential application in information encryption and encoding (Fig. 1b). This work not only establishes a paradigm for designing optical active MOF patterns with tailorable CPL performance, but also opens avenues for their application in next-generation miniaturized chiroptical devices, smart labels, and secure data storage technologies, addressing long-standing challenges in material science and optical engineering.

Results

Synthesis of a highly oriented MOF layer

$Cu(OH)_2$ nanowires (NWs) were synthesized in analogy to the previous procedure[37] (Fig. 2a), and subjected to morphological and structural analyses. Transmission electron microscopy (TEM) images revealed that the synthesized $Cu(OH)_2$ NWs exhibited typical diameters and lengths of around 10 nm and 1 μm, respectively (Supplementary Fig. 1a, b). Additionally, the high crystallinity and phase purity of the $Cu(OH)_2$ NWs were confirmed by X-ray diffraction (XRD) characterizations (Supplementary Fig. 2). The oriented $Cu(OH)_2$ NW films could be obtained by brush coating technique (Supplementary Fig. 1c), and subsequently acted as templates for heteroepitaxial growth of crystalline MOF patterns (Fig. 2a)[38]. The time-dependent Fourier transform infrared (FT-IR) analysis showed that the strong vibrations at 1567 cm^{-1} and 1397 cm^{-1} (attributed to -COOH symmetric and asymmetric vibrations) enhanced with the prolonged reaction time, indicating that $Cu(OH)_2$ NWs were completely converted to CuBDC MOF within 15 min (Supplementary Fig. 3). This was further confirmed by XRD characterizations. The (100) XRD peak intensity of CuBDC showed progressive enhancement with increasing reaction time (Supplementary Fig. 4), providing clear evidence for the formation of CuBDC MOF crystals. Moreover, the scanning electron microscope (SEM) characterizations were employed to monitor the transformation procedure (Supplementary Fig. 5). At the initial stage, well-oriented $Cu(OH)_2$ NWs could be observed. After immersing in the saturated ethanolic solution of H_2BDC for 2 min, MOF crystals orthogonal to $Cu(OH)_2$ NWs were detected. After immersing for 15 min, continuous MOF crystals could be prepared. SEM cross-section characterizations indicated that one layer of CuBDC crystalline MOF is about 1 μm thick and the layer thickness growed linearly while increasing the layer number (through cycles of brush painting and heteroepitaxial growth, see Supplementary Fig. 6). Energy dispersive X-ray analysis confirmed the homogeneously growth of MOF crystals films (Supplementary Fig. 7). Moreover, the intense profile of CuBDC MOF lattice parameter with respect to the azimuthal angle of the incident radiation showed two maxima at 0° and 180°, coincident with those of highly oriented $Cu(OH)_2$ NWs (Fig. 2b). All above results indicated that CuBDC MOF crystals were precisely oriented along $Cu(OH)_2$ NWs crystallographic directions, in accordance with previous reports[38]. Further, the obtained CuBDC MOF layer was highly anisotropic, confirmed by polarized ultraviolet-visible (UV-vis) absorbance (Fig. 2c) as well as polarized Raman characterizations (Supplementary Fig. 8). Interestingly, upon incorporation with various fluorescent dyes (including 9,10-Diphenylanthracene (DPA), Berberine, Congo red), the resultant oriented MOF layer exhibited anisotropic photoluminescent response, as displayed in Fig. 2d and Supplementary Fig. 9. An emission dichroic ratio ($R_F = P_{//}/P_{\perp}$) reached the maximum value of ~1.56, suggesting that the oriented MOF channel could orient encapsulated dye molecules and engender an anisotropic optical response. Further, we have employed single-molecule simulation to clarify the possible molecular orientation within MOF channels, by taking DPA as a model dye and using optimization at the PBE-D3 level. As shown in Supplementary Fig. 10, due to the size limitation, the DPA molecule has to be loaded in the diagonal fashion across the MOF channel, favoring anisotropic fluorescent response, which was in agreement with our experimental results and similar reports of Professor Falcaro and Takahashi groups[36,38].

Fabrication of twisted-stacking optical active MOF films with tailorable CPL properties

The critical step of fabricating twisted-stacking CuBDC MOF films is to macroscopically align another well-oriented MOF layer on top of the bottom dye-doped MOF layer in a twisted fashion. In practice, the well-oriented $Cu(OH)_2$ NWs layer was brushed clockwise or anticlockwise

https://doi.org/10.1038/s41467-025-65310-0

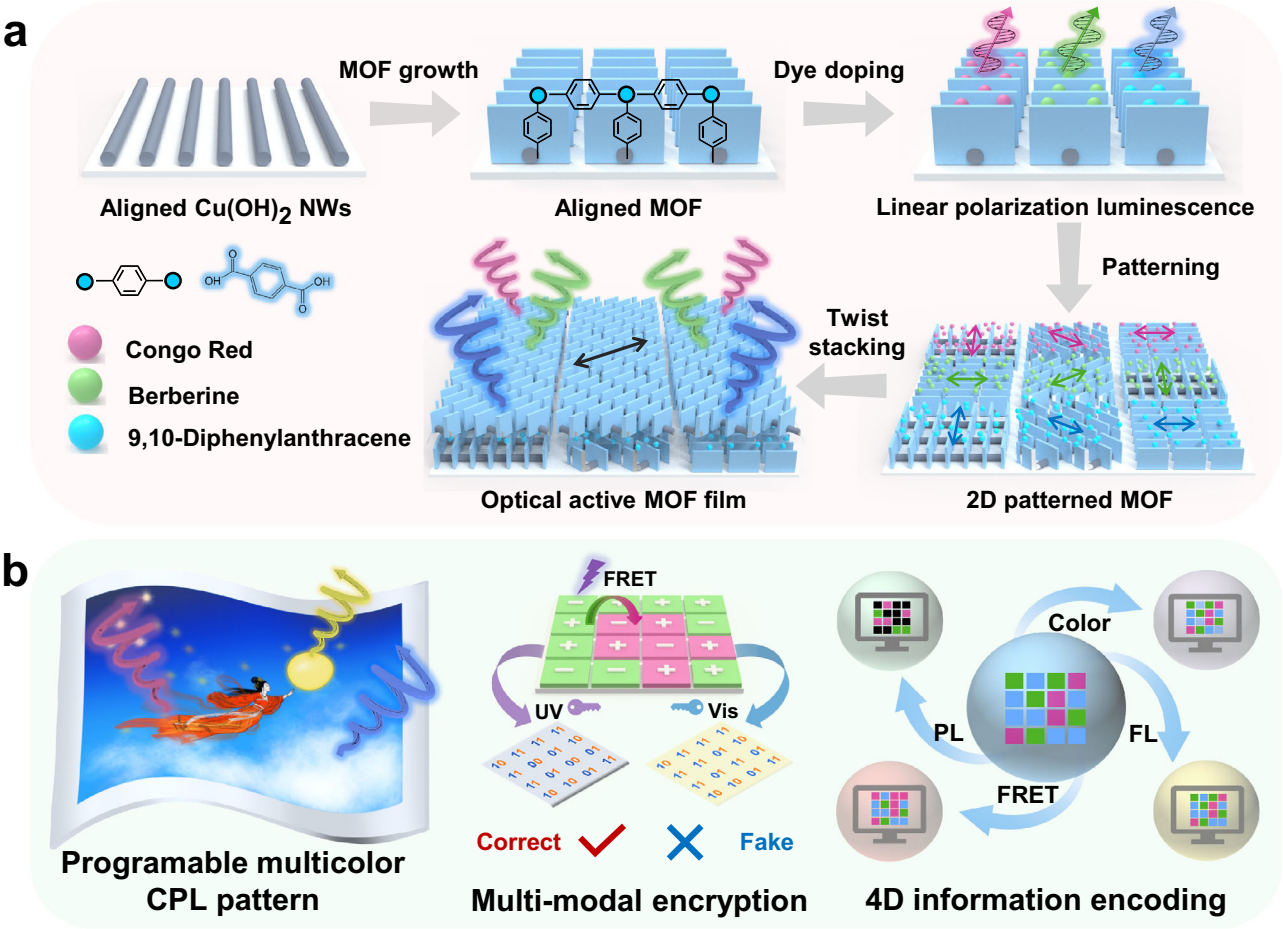

Fig. 1 | Schematic illustration of optical active MOF structure formation and its potential applications. a The fabrication protocol for twisted-stacking optical active MOF structure. **b** The potential applications in programmable full-color CPL patterns, multi-modal encryption, as well as 4D information encoding.

with a rotation angle to get left-handed (LH) or right-handed (RH) twisted-stacking structure, favoring the subsequent heteroepitaxial growth of the top MOF film with predesigned orientation. Specifically, the well-oriented $Cu(OH)_2$ NWs layer was prepared via brush coating strategy, following by heteroepitaxial growth of the MOF layer using the bottom $Cu(OH)_2$ NWs layer as the sacrificial template (Supplementary Fig. 11a). Then another well-oriented $Cu(OH)_2$ NWs layer was coated onto above well-oriented MOF layer via brush coating, in which the brush direction was kept constant while the bottom well-oriented MOF layer could be precisely rotated clockwise or anticlockwise to a certain angle. It should be noted here that the interlayer angle between two well-oriented $Cu(OH)_2$ NWs layers could be precisely modulated during the fabrication process. Subsequently, the top-aligned MOF layer could be prepared by a similar heteroepitaxial growth process using the top well-oriented $Cu(OH)_2$ NWs layer as the sacrificial template. MOF crystals were precisely oriented along the $Cu(OH)_2$ NWs direction; thus, the twist angle (θ) between the top and bottom MOF layers could be precisely controlled. SEM characterizations (Supplementary Fig. 11b) confirmed that the above twisted-stacking structure could be successfully fabricated. Moreover, SEM characterizations revealed that the thickness of the RH twisted-stacking MOF structures from RH-1 + 1(two numbers refer to the number of MOF layers in the bottom and upper, respectively) to RH-5 + 5 was about 2 μm, 4 μm, 6 μm, 8 μm, and 10 μm (Supplementary Fig. 12), respectively. Moreover, no visible morphology difference in SEM top surface images could be observed for different twisted-stacking MOF structures (Supplementary Fig. 13). Clearly, uniform MOF films could be obtained, indicating the excellent structural consistency and reproducibility for the twisted-stacking structures. The chiroptical properties of twisted-stacking optical active MOF films were investigated in detail by circular dichroism (CD) spectroscopy. As shown in Fig. 3a, large optical activities could be observed when the twist angle was either +45° or −45°, featuring the same bisignate CD signal characteristics but with opposite signs. The dissymmetric factor g_{abs} was determined to be 0.13/−0.15 (Supplementary Fig. 14), respectively. It should be noted here that no obvious CD signal could be detected for the single-layer of well-oriented MOF (Fig. 3a). As for twisted-stacking optical active MOF films, the obtained CD signal varied little when rotated or even flipped (Supplementary Fig. 15), indicating that the obtained chiroptical response resulted from the twisted-stacking structure, rather than linear dichroism (LD) or linear birefringence (LB) effect. A key structural parameter is the twist angle θ between the top and bottom layers. As expected, the magnitude of CD signals gradually decreased to zero when θ varied from 45° to 0°, and the CD signals inverted upon decreasing θ further to −45° (Supplementary Fig. 16). This θ dependence was in accordance with previous reports[28,30] and could be explained based on the principle of Jones Matrix[27]. We exploited the Jones Matrix presentation to predict the CD signals of such twisted-stacking MOF films. As shown in Supplementary Fig. 17, the good overall agreement of the calculation with the experimental results at various twist angles further confirmed that the optical activity should mainly originate from the twisted-stacking structure. Moreover, the number of twisted-stacking MOF layers greatly affected their chiroptical properties. As indicated in Fig. 3b, the CD response increased substantially when the number of layers increased from two (1 + 1) to six (3 + 3) with a fixed interlayer angle of 45°. The RH-3 + 3 film

https://doi.org/10.1038/s41467-025-65310-0

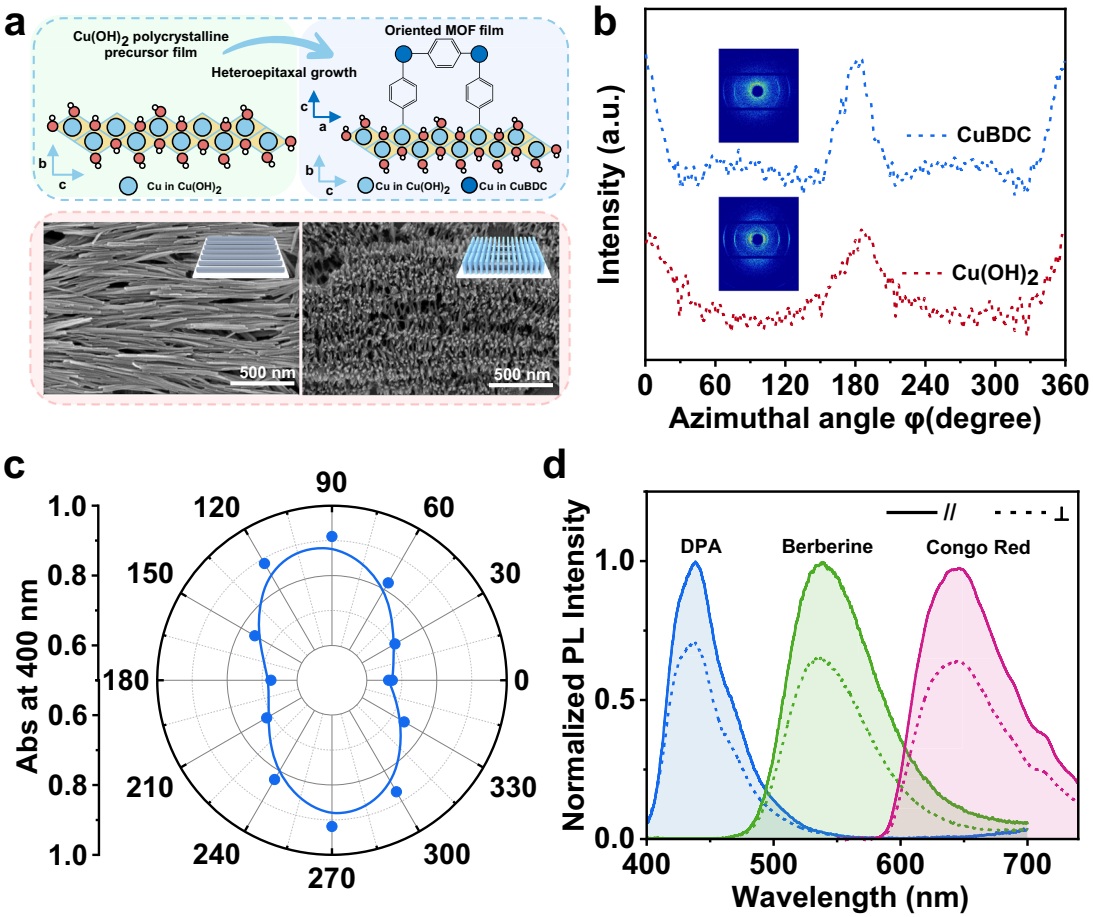

Fig. 2 | Characterizations of highly oriented MOF layer. a Schematic representation of the heteroepitaxial growth of CuBDC MOF film on aligned $Cu(OH)_2$ NW film and related SEM characterizations. The insets for the two lower panels respectively represent the schematic diagrams of $Cu(OH)_2$ NW film and MOF film. **b** 2D wide-angle X-ray diffraction of the two above films and their azimuth integration. **c** Polarized UV-vis absorption intensity at 400 nm of the oriented CuBDC film as a function of the relative rotation angle of the polarizer, ranging from 0° to 360°. **d** Polarized fluorescence spectra of dye-doped CuBDC films: DPA: λ_{ex} = 365 nm; Berberine: λ_{ex} = 365 nm; Congo red: λ_{ex} = 420 nm. The solid lines indicate the parallel light polarization to the transition dipole moment of the dye, and the dashed lines indicate the perpendicular light polarization to the transition dipole moment of the dye.

exhibited the highest CD signal (4238 mdeg and $|g_{abs}|$ value of ~0.15), almost 67 times larger than those for RH-1 + 1 films (Fig. 3b, Supplementary Figs. 18 and 19). However, when the number of MOF layers increased to eight (4 + 4), the CD response decreased, indicating that there was a limit in improving the CD signals. This is perhaps related to the unevenness of the twisted-stacking films.

As expected, no apparent CPL signal was observed for the single well-oriented MOF layer of fluorescent dye-doped MOF (Supplementary Fig. 20). While the twisted-stacking CuBDC optical active MOF films (3 + 3) exhibited CPL performance (Fig. 3c). To exclude possible LD effect, CPL characterizations were performed by rotating the obtained twisted-stacking MOF films about their normal axis in 45° intervals. As shown in Supplementary Fig. 21, the intensity of CPL signals for the left-handed twisted-stacking structure (LH-3 + 3) varied little upon rotation, indicating that the main origin of CPL signals should be ascribed to the twisted-stacking structure, rather than from LD or LB effects. Similarly, the obtained CPL signal was greatly dependent on the twist angle θ (Supplementary Fig. 22) and the number of the twisted-stacking MOF layers (Fig. 3d). The LH-3 + 3 film exhibited the highest CPL performance, and g_{lum} value could reach up to 0.16. For comparison, we have compiled a summary of the g_{lum} values for a selection of the most effective CPL-active MOF materials documented in the literature (Supplementary Fig. 23). Notably, our twist-stacking approach has achieved almost the highest g_{lum} value among MOF-based optical active materials. This is particularly crucial for their practical applications in programmable multicolor CPL patterns and information encryption, etc. It is worth noting that CPL intensity of the twist-stacking MOF films decreased upon heating to 90 °C, while upon cooling to room temperature, partial recovery of the original value was observed (Supplementary Fig. 24a). After five temperature cycles, over 65% CPL intensity remained. Besides, the films exhibited excellent humidity stability upon immersing into water (Supplementary Fig. 24b). The CPL intensity for the twist-stacking MOF films (kept under room temperature in air) remained almost unchanged over 1 month (Supplementary Fig. 25), indicating their excellent environmental stability.

Patterning of twisted-stacking optical active MOF films with arbitrary programmable CPL properties

More recently, optical active MOFs in the form of thin films offer disruptive potential to build solid-state devices, with broad implications in next-generation microelectronics, photonics, sensing, and biomedical application[39]. One of the key challenges to implement MOF chiral patterns in thin-film devices, especially those entailing miniaturized components, is the development of material-adapted patterning methods[33]. Herein, we presented a strategy to fabricate programmable

https://doi.org/10.1038/s41467-025-65310-0

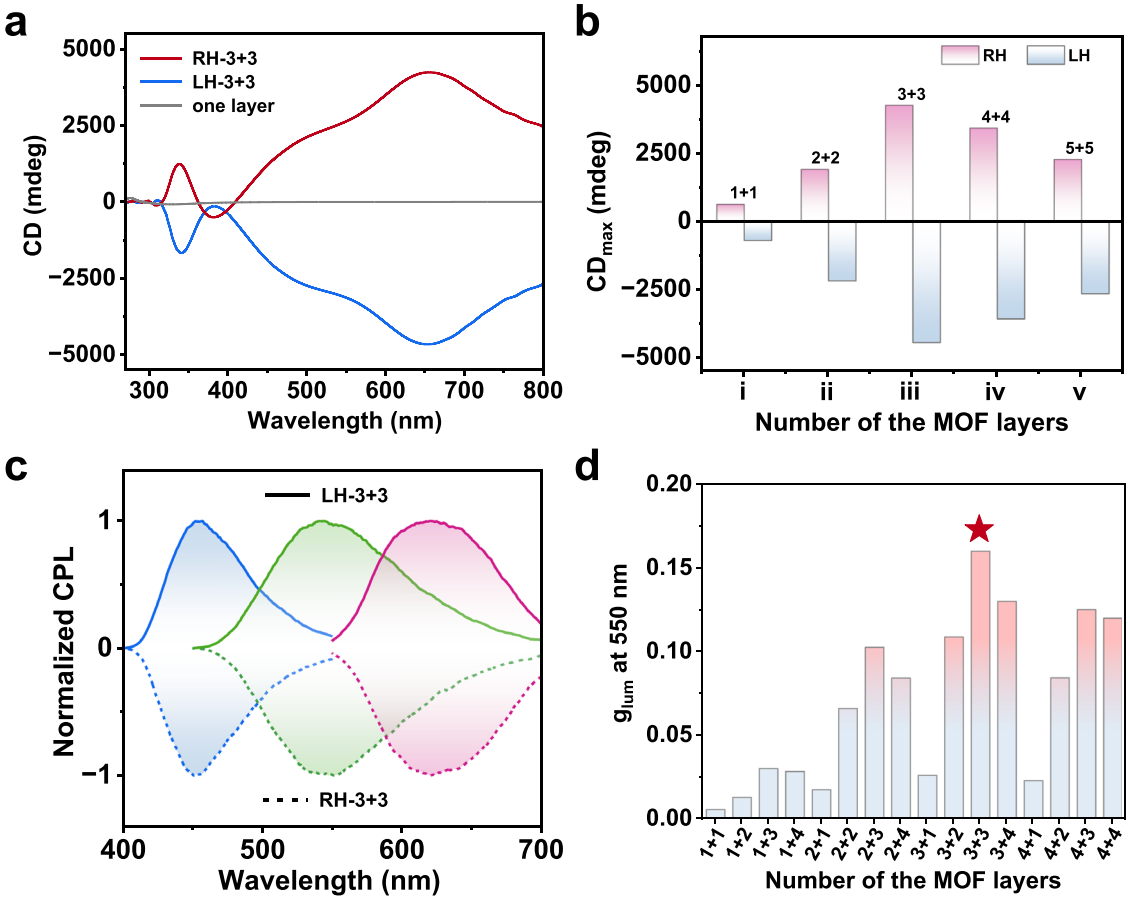

Fig. 3 | Chiroptical properties of the twisted-stacking MOF films. a CD response of the optical active MOF films with a fixed inter-angle of 45° and a single-layer of well-oriented MOF film. RH-3 + 3 = right-handed with 6 layers of MOF assembly. **b** CD maximum value of the optical active MOF films with a different number of layers and handedness with a fixed inter-angle of 45°. **c** Normalized CPL spectra of different dyes doped optical active MOF films (solid lines represent LH-3 + 3, dashed lines represent RH-3 + 3). **d** g_{lum} of the Berberine doped optical active MOF films with a different number of layers, in which the twisted-stacking angle of the two layers is +45°.

MOF CPL patterns (Fig. 4a). This strategy allowed us to generate chirality gradients and CPL gradient distributions in the above MOF films. As shown in Fig. 4b (left panel), by either varying the concentration of dye (1–5) or the orientation direction of MOF patterns of the bottom layer (5–9), a matrix of square patches of MOF CPL patterns with tailorable CPL performance could be achieved. As proven by the CPL characterization shown in Fig. 4b (middle panel), the CPL intensity increased as the concentration of Berberine increased, accompanied by a simultaneous enhancement in fluorescence intensity (Supplementary Figs. 26 and 27). In another circumstance, while keeping the overall fluorescence intensity constant, a gradient in CPL could be achieved by simply varying the orientation direction of MOF patterns of the bottom layer, as shown in Fig. 4b (right panel) and Supplementary Figs. 28 and 29. Interestingly, upon loading with different phosphorescent dyes, for instance, 11,12-dihydroindolo[2,3-a] carbazole (ICz) and 7H-dibenzo[c,g]-carbazole (DBCz), multicolor circularly polarized phosphorescence (CPP) MOF patterns could be generated, as shown in Fig. 4c. In addition, above MOF CPL patterns could also be prepared on a flexible polydimethylsiloxane (PDMS) substrate, which offered excellent flexibility and mechanical deformability. Importantly, upon folding, bending, or twisting operations, both fluorescence and CPL signals of these curved MOF/PDMS films were virtually indistinguishable (Fig. 4d), indicating that mechanical deformation of these flexible MOF CPL patterns would not compromise their chiroptical performance. To sum up, we envisage here that precisely programmable, optical active MOF films with patterning could be fabricated, which would promote the integration of MOF CPL components into miniaturized chiroptical devices.

Multi-modal encryption based on photo-responsive CPL switching

Stimuli-responsive CPL patterns are highly attractive due to their potential applications in chiroptical electronic devices and multi-dimensional information encryption[40,41]. Here, we demonstrated photo-responsive MOF CPL patterns (including color and handedness) based on the dynamically tunable fluorescence resonance energy transfer (FRET) process by utilizing the stretched polyvinyl alcohol (PVA) layer as the phase retardation layer[42] (Fig. 5a). As expected, the MOF/Berberine+Spiropyran/PVA hybrid films emitted strong green fluorescence and positive CPL signal with a high g_{lum} (-0.4) (Fig. 5b). Moreover, the phase retardation of the PVA layer could be precisely regulated by varying the strain or thickness of PVA layer (Supplementary Fig. 30), leading a dynamical CPL modulation or even chirality inversion (CPL signal from positive to negative), which were in accordance with previous report[43]. Upon exposure to 365 nm UV irradiation for 1 min, the Spiropyran units transferred from the colorless ring-closed spirocyclic (SP) form to the colored ring-opened merocyanine (MC) form, resulting in the emergence of red fluorescence due to the FRET between Berberine and Spiropyran units in MC form (Supplementary Fig. 31). In addition to the red-shifted emission, the CPL signal was also inversed (Fig. 5b), which should be ascribed to the wavelength-dependent phase retardation behavior of the transparent

https://doi.org/10.1038/s41467-025-65310-0

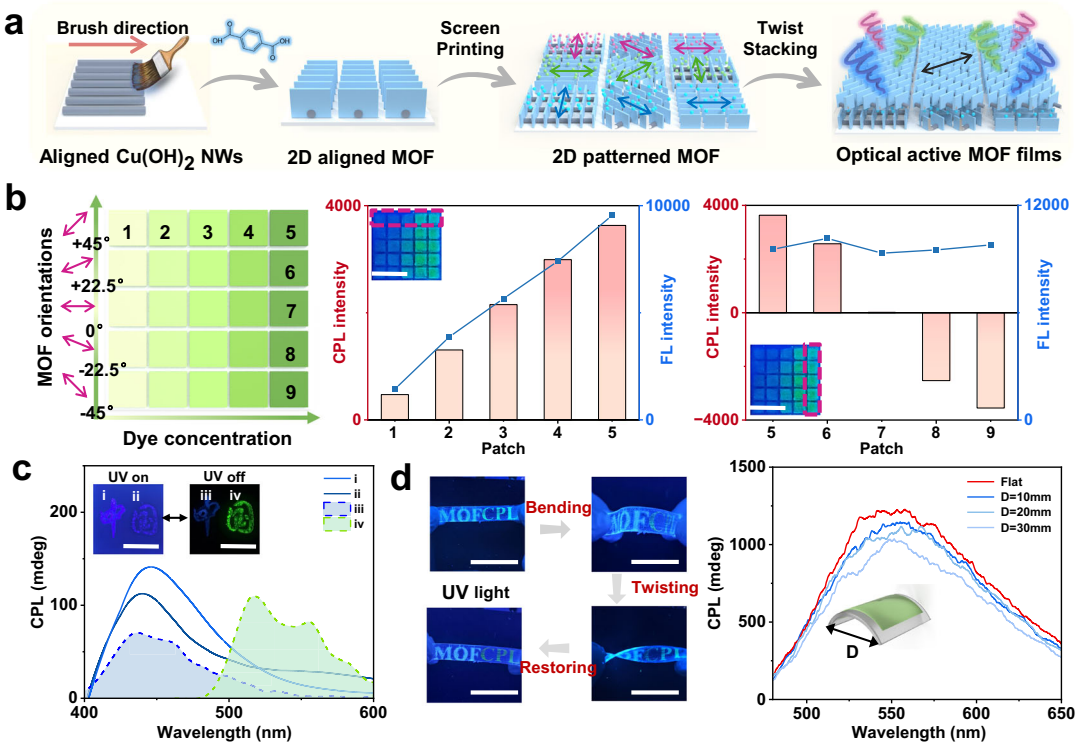

Fig. 4 | Fabrication process of patterned optical active MOF films with tunable CPL. a Schematic diagram of the arbitrary programmable CPL pattern process for twisted-stacking structure of the MOF via the combination of screen printing and brush painting process. **b** A matrix of MOF films with tailorable chirality. The patches in each row were doped with different concentrations of Berberine and in each column with varying orientations of MOF, resulting in a 2D matrix of MOF patches, each owns characteristic chirality and intensity. The inset shows the fluorescence image of the MOF film matrix viewed with naked eyes. **c** The CPL spectra of different distinct regions of the different patterned optical active MOF films. The insets show the fluorescence and phosphorescence images of the patterned MOF film viewed with naked eyes. **d** The fluorescence images of the MOF film under different deformation conditions such as flat laying, bending, twisting, and restoring, and CPL spectra of MOF films on several semicylindrical surfaces with different curvatures (D = 10 mm, 20 mm, 30 mm, and flat as a comparison) using flexible PDMS films as support. Scale bar for the fluorescent patterns: 1 cm.

anisotropic PVA layer. Based on Jones Matrix and the simulated calculation[42], the phase retardation ϕ of transparent anisotropic PVA layer at 530 nm was about −121° with $\sin\phi > 0$ (Supplementary Fig. 32), leading to a positive CPL signal. While the phase retardation ϕ at 650 nm was about −238° with $\sin\phi < 0$, resulting in negative CPL signals. It should be noted here that after irradiation with 445 nm light for 1 min, the MC form of Spiropyran transferred back to the SP form, the hybrid films turned back to green, and their resulting CPL signal returned back to its initial state (before UV irradiation), indicating that the photo-triggered CPL modulation (including color switching and the handedness inversion) was completely reversible. More importantly, the CPL signal of the hybrid film showed excellent cyclability after alternative UV and visible irradiations (Supplementary Fig. 33).

Recently, multimode independent information encoding has attracted increasing attention due to its ability to enhance the capacity and security of information encoding[44]. It was anticipated that multi-dimensional information encoding could be designed based on the above multi-responsive CPL pattern. Therefore, we developed a multifunctional information encryption system by combining the widely acclaimed 2D color code with the promising CPL signal. As illustrated in Fig. 5c, composite films doped with different types of fluorescent dyes were fabricated into a 4 × 4 pixel array. Specifically, the well-oriented MOFs layer doped with different dyes was fabricated by a multistage screen-printing process. The layer composition within regions i, ii, and iii was the MOFs layer doped with Berberine, Congo red, and the mixture of Berberine and Spiropyran, respectively. Then the individual pixel in Fig. 5c was constructed by overlaying another oriented PVA layer onto the above multi-colored fluorescent MOFs layer with a different twist angle (45° or −45°). The film squares emitted either green or red color, which allowed various information to be displayed. To demonstrate 2D encoding with high-security encryption, we employed the fluorescence and the CPL signal as Channel 1 and Channel 2, respectively, to create a binary coding system. For Channel 1, it was encoded as "1" when green fluorescence was present, while "0" for red fluorescence. In the case of Channel 2, "1" or "0" was encoded when the CPL sign was positive or negative, respectively. The digits obtained from Channels 1 and 2 were interleaved to obtain a new digital code for the combined information. These digits could be further converted into hexadecimal (HEX) and decoded through the Chinese Internal Code Specification (GBK). As expected, meaningless fake information ("况莽") was obtained at the initial state. However, upon UV irradiation, the encrypted information "科学" could be correctly read out. After heating or irradiation with visible light, the encrypted information would be hidden again, and only fake information could be decoded, indicating their potential application in safeguarding valuable and authentic information. It should be noted here that after decoding, the encrypted information could be easily destroyed by immerging the film squares into an acetic solution, favoring high-level secure information encryption.

4D information encoding

In recent years, 4D information encoding has emerged as a transformative paradigm in data security, garnering substantial scientific interest owing to its potential for simultaneously augmenting information storage capacity while ensuring robust cryptographic protection[45]. As mentioned above, upon varying the doped dyes or the orientations of the aligned MOF arrays, it was possible to obtain CPL patterns with desired color and chirality distribution independently.

https://doi.org/10.1038/s41467-025-65310-0

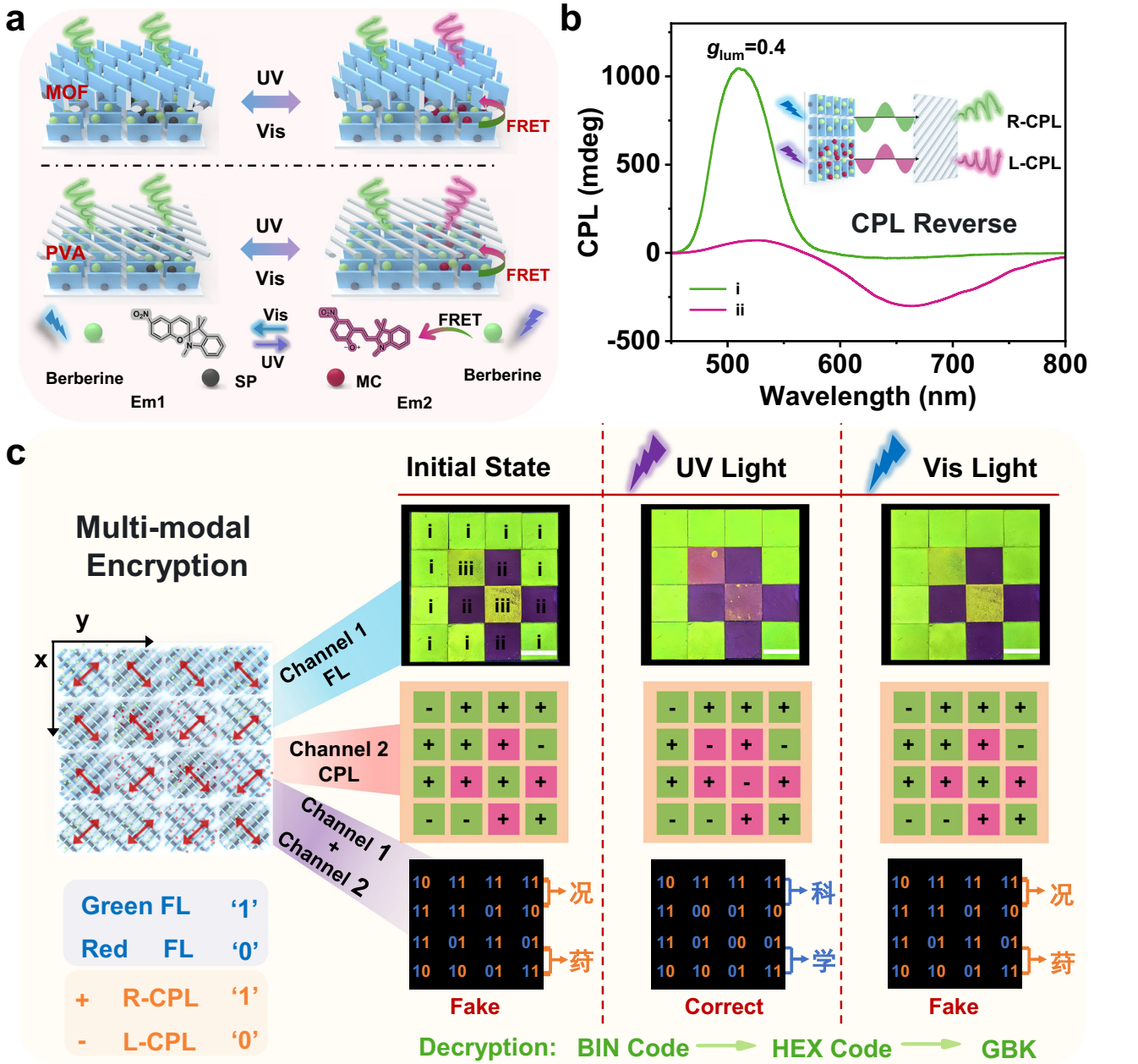

Fig. 5 | Multi-modal encryption of the twisted-stacking MOF films. a Schematic illustration of photo-responsive CPL switching based on the FRET between Berberine and Spiropyran units in MC form. **b** CPL spectra of MOF/Berberine+Spiropyran /PVA hybrid film were obtained (i) before and (ii) after UV irradiation, upon excitation at 445 nm and 365 nm, respectively. **c** Fluorescence and CPL signals of the pixel array (the bottom layer consists of the MOF films with different orientations (the red arrows indicate the orientation direction), and the upper layer was made of the stretched PVA oriented along the x-axis.) acquired at UV and visible irradiation, in which the fluorescence images served as Channel 1, and CPL information served as Channel 2. Scale bar for the fluorescent patterns: 1 cm.

Therefore, we further validated the usage of them by performing information encoding, as shown in Fig. 6. Specifically, seven-segment multi-colored fluorescent/phosphorescent MOF/PVA hybrid films were fabricated following a similar preparation process in Fig. 5. In the regions i and vi, the LH and RH twisted-stacking structures of MOF/DBCz/PVA films were fabricated, respectively. In the regions ii and iii, the LH twisted-stacking structures of MOF/Berberine/PVA films were fabricated, while the RH twisted-stacking structures of MOF/Berberine/PVA films were fabricated in the region iv. In the region v and vii, the RH and LH twisted-stacking structures of MOF/Berberine+Spiropyran/PVA films were fabricated, respectively. Seven patches of optical active MOF films with independent color and CD/CPL signal could be assembled; together they could compile a symbol for American Standard Code for Information Interchange (ASCII) as the cryptographic algorithm. Green and other colors were defined as "1" and "0," respectively, for the apparent encoding, while a positive signal ($CD_{530\ nm}$ value or CPL value > 0) and a negative signal ($CD_{530\ nm}$ value or CPL value < 0) were defined as "1" and "0," respectively, for the covert encoding. Thus, the first layer of encoded information could be read by analyzing both the color and CD/CPL signal of the designed area (Figs. 6a, b), Subsequently, binary and hexadecimal ASCII were used for the second and third decryptions of different areas, and the combination of numbers and letters obtained from hexadecimal decoding through the GBK code encoding yielded the correct information—Chinese characters. As expected, the encoded information could only be correctly displayed when both the color and chirality of

https://doi.org/10.1038/s41467-025-65310-0

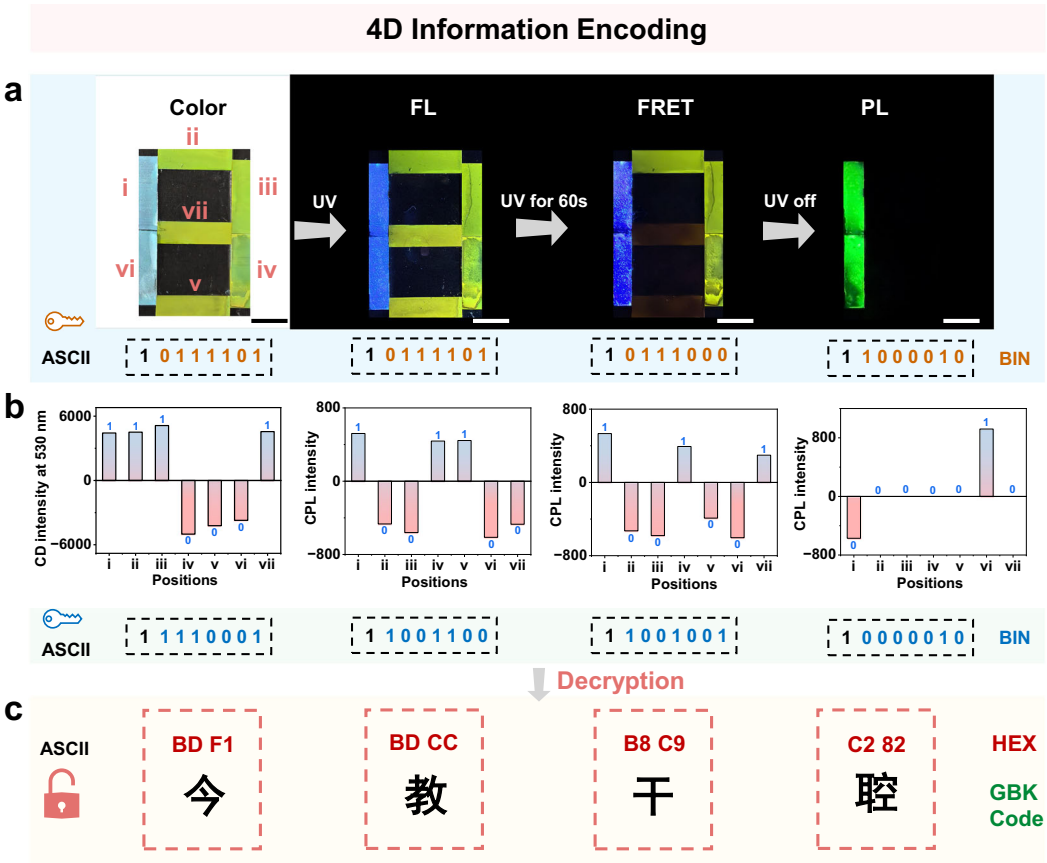

Fig. 6 | Design and concept of 4D information encryption and decryption. **a** Photos of the MOF films doped with different dyes (i, vi: DBCz; ii, iii, iv: Berberine; v, vii: Berberine and Spiropyran). This color code displayed four different color matrices under daylight, UV excitation, UV irradiation for 1 min, and after removal of the excitation light, respectively. **b** CD and CPL intensity of four different contexts. **c** The decryption result of 4D information encoding. Scale bar for the patterns: 1 cm.

the encoding pattern were read out. For instance, when interpreting this combination code, the overt code could be read as "3" with visual color difference, which is binary ASCII "0111101," and the covert code could be obtained through CD characterization, with binary ASCII "1110001." Decrypting both codes into hexadecimal ASCII resulted in the combinations "BD" and "F1," then cross-integrated and decrypted through GBK encoding, yielding the code for the Chinese character "今" (Fig. 6c), achieving multiplex anti-counterfeiting decryption. Consequently, programmable MOF films functionalized with distinct dyes and controlled orientations could serve as orthogonal encryption keys, enabling multidimensional information encoding within planar architectures. This advanced encryption paradigm fundamentally surpassed conventional encryption limitations. The enhanced security arose from the necessity to resolve massive combinatorial datasets during decryption, under the condition of the uncertain cipher.

Discussion

In summary, we have developed optical active MOF patterns with tailorable CPL performance and exceptional stimuli-responsive properties. The fabrication of 2D programmable MOF patterns with highly oriented crystalline structures is achieved by combining brush coating, bottom-up heteroepitaxial growth, and twisted-stacking techniques. With the aid of color and CD/CPL signals, stimuli-responsive multicolor optical active MOF patterns are easily constructed with on-demand tunability, conferring a dynamic expression of information platform for potential applications of multi-modal encryption and 4D information encoding. This work not only advances the engineering of multifunctional optical active MOF patterns but also creates paradigms for understanding tunable light-matter interactions and designing next-generation stimuli-responsive chiroptical programmable architectures, offering transformative potential across photonics, sensing, and information security fields.

Our results show convincingly that optical active MOFs films with tunable CPL properties, which can be precisely fabricated via the combination of bottom-up heteroepitaxial growth and twisted-stacking strategy. Nevertheless, the obtained g_{lum} value of the optical active MOFs films is only 0.4, limiting their practical applications. There is still plenty of room for improvement in g_{lum} value as well as the inverse designability. In the future, we will employ the data-driven machine learning techniques to optimize the composition and the detailed preparation procedure of the twisted-stacking MOF structures, which can offer more freedom to amplify their optical activity to acquire high g_{lum} value, also may open doors to inverse design and customized manufacturing of optical active MOFs films with target functionality.

Methods

Materials

Sodium hydroxide (NaOH), ammonium hydroxide (NH_4OH), copper sulfate pentahydrate ($CuSO_4{\cdot}5H_2O$), ethanol (EtOH), 1-Hexanol, Terephthalic acid (H_2BDC), 9,10-Diphenylanthracene (DPA), Berberine, Congo red, 7H-dibenzo[c,g]-carbazole (DBCz), 11,12-dihydroindolo[2,3-a] carbazole (ICz) were purchased from Aladdin. Polydimethylsiloxane (PDMS, Sylgard 184, which contains component A (base glue) and component B (curing agent)) was purchased from Dow Corning. 1,3,3-Trimethylindolino-6′-nitrobenzopyrylospiran was

purchased from Sigma-Aldrich. All of the above chemicals were used without further purification. PVA with an acetalization degree of 98–99% and a thickness of 80 μm was purchased from Anhui Wanwei High-Tech Material Industry Co., Ltd. The weight-averaged molecular weight (Mw) was approximately 43 kg/mol, with a polydispersity index of 3.8. Deionized (DI) water was used for experimental procedures and solution preparation (18 MΩ·cm^{-1}).

Synthesis of $Cu(OH)_2$ NWs

$Cu(OH)_2$ NWs were synthesized according to the approach of ref. 37. To obtain pure copper hydroxide, the synthesis was performed with a 12 M NaOH aqueous solution. First, 30 ml of 0.15 M NH_4OH solution was added dropwise to 100 ml of 0.04 M $CuSO_4{\cdot}5H_2O$ aqueous solution. After stirring for 5 min, 6 ml of 12 M NaOH aqueous solution was added dropwise to the blue solution under stirring. After adding NaOH aqueous solution, the solution became milky blue. The solution was stirred for 1 h at room temperature and then held at 40 °C for 30 min without stirring. The milky blue powders were centrifuged and washed with water and ethanol. The resultant copper hydroxide NWs (3 g) were dispersed in ethanol (30 ml) and stored for future use.

Synthesis of oriented MOF on $Cu(OH)_2$ NWs

The $Cu(OH)_2$ NWs initially dispersed in ethanol were subsequently re-dispersed in n-hexanol at a concentration of 0.2 g/ml. A quartz substrate was positioned on a heating pad maintained at 40 °C, and the copper hydroxide nanowires were carefully deposited onto the quartz surface using a brush to form well-oriented copper hydroxide nanowire films. The conversion from $Cu(OH)_2$ to CuBDC was performed at room temperature by immersing the obtained $Cu(OH)_2$ film in a saturated ligand solution (mixture of 3.6 ml water, 9.34 ml ethanol, and 0.1 g H_2BDC). After 15 min, the product was removed from the solution and washed with water and ethanol, and then dried under air.

Fabrication of the 2D patterned MOF

The orientation direction of the $Cu(OH)_2$ NWs in different regions of the quartz substrate could be precisely controlled by rotating above substrate to a certain rotation angle, and a 2D pattern of the well-oriented $Cu(OH)_2$ NWs could be prepared via a multistage brush coating process. Subsequently, the above 2D $Cu(OH)_2$ NWs patterned film was immersed in a saturated ligand solution (3.6 ml of water, 9.34 ml of ethanol mixture, 0.1 g of H_2BDC) for the heteroepitaxial growth of 2D patterned MOF films. Then, different dye solutions (including 9,10-Diphenylanthracene, Berberine, and Congo red in ethanol solutions, 1 mg/ml) could be sprayed onto different regions of the prepared 2D patterned MOF films by a multistage screen-printing process, favoring the construction of a 2D patterned multi-colored fluorescent MOFs layer, as illustrated in Figs. 1a and 4a.

Fabrication of twisted-stacking MOF films with tailorable CPL properties

The well-oriented $Cu(OH)_2$ NWs layer was prepared via a brush coating strategy, with the brush coating speed of ~2 cm/s (the brush direction was kept constant). Then well-oriented $Cu(OH)_2$ NWs film was immersed in a saturated ligand solution (3.6 ml of water, 9.34 ml of ethanol mixture, 0.1 g of H_2BDC), and the aligned MOF layer can be prepared via heteroepitaxial growth strategy using the bottom $Cu(OH)_2$ NWs layer as the sacrificial template. Then another well-oriented $Cu(OH)_2$ NWs layer was coated onto the above well-oriented MOF layer via brush coating, in which the brush direction was kept constant while the bottom well-oriented MOF layer could be precisely rotated clockwise or anticlockwise to a certain angle. It should be noted here that the interlayer angle between two well-oriented $Cu(OH)_2$ NWs layers could be precisely modulated during the fabrication process. Subsequently, the top-aligned MOF layer could be prepared by a similar heteroepitaxial growth process using the top well-oriented $Cu(OH)_2$ NWs layer as the template. MOF crystals were precisely oriented along the $Cu(OH)_2$ NWs direction; thus, the twist angle (θ) between the top and bottom MOF layers could be precisely controlled. The second well-oriented MOF layer with a certain twist angle was deposited onto the surface of the above MOF/dye patterns and acts as the phase retardation layer to generate CPL response based on a Jones Matrix mechanism.

Fabrication of twisted-stacking MOF/PVA hybrid films with tailorable CPL properties

For the case of multi-modal encryption and information encoding, the stretched PVA layer (the thickness of PVA is 80 μm and the strain is 100%) was employed as the phase retardation layer instead of the upper oriented MOF layer to achieve dynamical CPL inversion.

Computational methods

First-principles calculations were performed using the Vienna Ab initio Simulation Package based on spin-polarized density functional theory (DFT). The Perdew-Burke-Ernzerhof (PBE) exchange-correlation functional within the generalized gradient approximation was employed. The projector augmented wave method was used to describe the electron-ion interactions, with a plane-wave cutoff energy of 400 eV.

Electronic structure calculations were carried out with Gaussian smearing (ISMEAR = 0) using a smearing width of 0.05 eV. The electronic self-consistency convergence criterion was set to 10^{-5} eV (EDIFF), with a minimum of five electronic steps (NELMIN) and a maximum of 300 steps (NELM). Spin-polarized calculations were performed (ISPIN = 2) with an initial magnetic moment configuration of 1.0 μB assigned to 24 atoms, while the remaining atoms (114 + 218 + 96 = 428 atoms) were initialized with zero magnetic moments.

Structural optimizations were performed using the conjugate gradient algorithm (IBRION = 2) with a force convergence criterion of 0.02 eV/Å (EDIFFG). The ionic relaxation was allowed for atomic positions only (ISIF = 2), keeping the cell shape and volume fixed. A maximum of 1000 ionic steps (NSW) was permitted with a step width scaling factor (POTIM) of 0.2. Van der Waals interactions were included using the DFT-D3 method with Becke-Johnson damping (IVDM = 12).

Symmetry was turned off (ISYM = 0) during the calculations to allow for proper treatment of magnetic configurations and structural relaxations. All calculations were performed with automatic real-space projection (LREAL = Auto) to improve computational efficiency.

Characterizations

All films were investigated in the solid state. UV-vis spectra were recorded using a Shimadzu UV-2700 spectrophotometer, FT-IR spectra were recorded on a Bruker TENSOR II spectrometer, and CD spectra were recorded using a JASCO J-1500 spectropolarimeter. Circularly polarized photoluminescence was measured using a JASCO CPL-300 spectrometer. Fluorescence spectra of the films were obtained on a Hitachi fluorescence spectrometer F-4600. CPP properties were recorded on a home-made analytical device by combining a fluorospectrophotometer (Hitachi F-4700) with a left-handed/right-handed circularly polarized filter (L/R-CPF)[46]. We can obtain the CPP value through a simple calculation: CPP = (I_L–I_R), where I_L and I_R are the recorded phosphorescence intensity passing through L-CPF and R-CPF, respectively. Raman spectra were measured by a spectrometer (LabRAM HR Evolution). The morphology of the oriented $Cu(OH)_2$ NWs and oriented CuBDC was characterized by high-resolution TEM (Hitachi HT-7650 electron microscope), scanning electron microscopy (SEM, Merlin Compact, Carl Zeiss, Jena, Germany, and Schottky Field Emission Scanning Electron Microscope, GeminiSEM 500). The samples for electron microscopy analysis were prepared by brush-casting a dilute solution of the $Cu(OH)_2$ NWs onto the substrate, either on ultrathin carbon-coated copper grids for TEM analysis or onto a clean

glass wafer for SEM. In situ WAXS measurements were carried out on a synchrotron radiation X-ray scattering station with a radiation wavelength of 0.154 nm and a Mar 345 image plate as a detector in the National Synchrotron Radiation Laboratory, Hefei, China. The sample-to-detector distance for WAXS was 323 mm. The Fit 2D software package was used to analyze the two-dimensional (2D) WAXS patterns. The air background was subtracted from the 2D scattering patterns. XRD spectroscopy analysis (XRD, MiniFlex II, Rigaku, Tokyo, Japan) was performed with a Cu target ($\lambda = 1.540598$ Å) at a generator voltage of 30 kV and a scanning rate of 0.05° per minute.

Data availability

The authors declare that all relevant data supporting the findings of this study are available within this article and its supplementary information. All data are available upon request. Source data are provided with this paper.

References

1. Xiao, Y. H. et al. Chiral metal–organic cluster induced high circularly polarized luminescence of metal-organic framework thin film. *Adv. Funct. Mater.* **32**, 9078–9144 (2022).
2. Senkovska, I., Bon, V., Mosberger, A., Wang, Y. & Kaskel, S. Adsorption and separation by flexible MOFs. *Adv. Mater.* **37**, 2414724 (2025).
3. Jo, Y. M. et al. MOF-based chemiresistive gas sensors: toward functionalities. *Adv. Mater.* **35**, 2206824 (2023).
4. Yao, M. S. et al. Van der Waals heterostructured MOF-on-MOF thin films: cascading functionality to realize advanced chemiresistive sensing. *Angew. Chem. Int. Ed.* **58**, 14915–14919 (2019).
5. Zou, W., Li, Q., Wu, Q., Zhang, Z. & Zhou, Y. Bifunctional Dy-MOF for efficient electrochemical detection and photocatalytic reduction of Cr(VI). *Chem. Eng. J.* **505**, 159428 (2025).
6. Ali, A. et al. Heteropoly ionic liquid functionalized MOF-Fe: synthesis, characterization, and catalytic application in selective acetalization of glycerol to solketal as a fuel additive at room temperature, solvent-free conditions. *Precis. Chem.* **1**, 485–496 (2023).
7. Li, W. et al. Scalable multifunctional MOFs-textiles via diazonium chemistry. *Nat. Commun.* **15**, 5297 (2024).
8. Zhou, Z. et al. Porphyrinic MOF film for multifaceted electrochemical sensing. *Angew. Chem. Int. Ed.* **60**, 20551–20557 (2021).
9. Yang, Y. et al. Unexpected "spontaneous" evolution of catalytic, MOF-supported single Cu(II) cations to catalytic, MOF-supported Cu(0) nanoparticles. *J. Am. Chem. Soc.* **142**, 21169–21177 (2020).
10. Li, M. et al. Zirconium-based metal-organic frameworks for photocatalytic CO_2 reduction. *Precis. Chem.* **3**, 424–450 (2025).
11. Wang, X., Zhang, H., Li, J. & Zou, G. Monitoring of sweat pH and dual-mode anti-counterfeiting from metal-organic framework-based multifunctional gel. *Chin. J. Chem.* **42**, 491–498 (2024).
12. Zhang, Y. et al. Tunable chiral metal organic frameworks toward visiblelight-driven asymmetric catalysis. *Sci. Adv.* **3**, e1701162 (2017).
13. Chen, T., Li, H., Shi, X., Imbrogno, J. & Zhao, D. Robust homochiral polycrystalline metal–organic framework membranes for high-performance enantioselective separation. *J. Am. Chem. Soc.* **146**, 14433–14438 (2024).
14. Zheng, H. et al. Dual-ligand chiral MOFs exhibiting circularly polarized room temperature phosphorescence for anti-counterfeiting. *Sci. China Chem.* **68**, 3064–3070 (2025).
15. Zhang, C. et al. Enantiomeric MOF crystals using helical channels as palettes with bright white circularly polarized luminescence. *Adv. Mater.* **32**, 2002914 (2020).
16. Gong, W., Chen, Z., Dong, J., Liu, Y. & Cui, Y. Chiral metal-organic frameworks. *Chem. Rev.* **122**, 9078–9144 (2022).
17. Zhang, H. et al. Synthesis strategies, preparation methods, and applications of chiral metal-organic frameworks. *Chem. Eur. J.* **30**, e202401091 (2024).
18. Xiao, Y.-H. et al. Inducing circularly polarized luminescence by confined synthesis of ultrasmall chiral carbon nanodot arrays in pyrene-based MOF thin film. *ACS Nano* **17**, 19136–19143 (2023).
19. Geng, L. et al. Solution-processable metal-organic framework featuring highly tunable dynamic aggregation states. *Adv. Mater.* **37**, 2415511 (2024).
20. Wang, J. Y. et al. Stepwise amplification of circularly polarized luminescence in chiral metal cluster ensembles. *Adv. Sci.* **10**, 2207660 (2023).
21. Wang, X. Z. et al. Highly boosting circularly polarized luminescence of chiral metal–imidazolate frameworks. *Adv. Sci.* **10**, 2207333 (2023).
22. Sui, L. et al. Breaking mirror circularly polarized luminescence of chiral metal–organic frameworks by high-pressure stimulation. *CCS Chem.* **5**, 2215–2224 (2023).
23. Yang, X.-X. et al. Chiral liquid crystalline metal–organic framework thin films for highly circularly polarized luminescence. *J. Am. Chem. Soc.* **146**, 16213–16221 (2024).
24. Zhao, T., Han, J., Shi, Y., Zhou, J. & Duan, P. Multi-light-responsive upconversion-and-downshifting-based circularly polarized luminescent switches in chiral metal–organic frameworks. *Adv. Mater.* **33**, 2101797 (2021).
25. Lv, J., Yang, X. & Tang, Z. Rational design of all-inorganic assemblies with bright circularly polarized luminescence. *Adv. Mater.* **35**, 2209539 (2022).
26. Wen, L. et al. Amplification and dynamic control of circularly polarized luminescence in poly (vinyl alcohol)/CdSe@CdS nanorod assembly twisted-stacking hetero-structures. *Adv. Opt. Mater.* **12**, 2301308 (2023).
27. Xie, Y. et al. Flexible, programmable, chiroptical polymer films of twisted stacking layers for circular polarization-based multiplex color display. *Adv. Opt. Mater.* **10**, 2102197 (2021).
28. Lv, J. et al. Gold nanowire chiral ultrathin films with ultrastrong and broadband optical activity. *Angew. Chem. Int. Ed.* **56**, 5055–5060 (2017).
29. Lv, J. et al. Biomimetic chiral photonic crystals. *Angew. Chem. Int. Ed.* **58**, 7783–7787 (2019).
30. Chen, L. et al. Chiral self-assembled film from semiconductor nanorods with ultra-strong circularly polarized luminescence. *Angew. Chem. Int. Ed.* **60**, 26276–26280 (2021).
31. Bo, R. et al. Paper-like writable nanoparticle network sheets for mask-Less MOF patterning. *Adv. Funct. Mater.* **32**, 2100351 (2021).
32. Brandner, L. A. et al. Ordered transfer from 3D-oriented MOF superstructures to polymeric films: microfabrication, enhanced chemical stability, and anisotropic fluorescent patterns. *Adv. Mater.* **36**, 2404384 (2024).
33. Tian, X. et al. Crosslinking-induced patterning of MOFs by direct photo- and electron-beam lithography. *Nat. Commun.* **15**, 2920 (2024).
34. Gartner, Z. J. & Hu, J. L. Guiding tissue-scale self-organization. *Nat. Mater.* **20**, 2–9 (2020).
35. Tu, M. et al. Direct X-ray and electron-beam lithography of halogenated zeolitic imidazolate frameworks. *Nat. Mater.* **20**, 93–99 (2020).
36. Velásquez-Hernández, M.dJ. et al. Fabrication of 3D oriented MOF micropatterns with anisotropic fluorescent properties. *Adv. Mater.* **35**, 2211478 (2023).
37. Seo, S. et al. Low-temperature synthesis of CuO-interlaced nanodiscs for lithium ion battery electrodes. *Nanoscake Res. Lett.* **6**, 397 (2011).

38. Falcaro, P. et al. Centimetre-scale micropore alignment in oriented polycrystalline metal–organic framework films via heteroepitaxial growth. *Nat. Mater.* **16**, 342–348 (2016).
39. Kulachenkov, N. et al. MOF-based sustainable memory devices. *Adv. Funct. Mater.* **32**, 2107949 (2021).
40. Qiao, J., He, Y., Lin, S., Fan, Q. & Guo, J. A photoswitchable circularly polarized luminescent cholesteric superstructure: direct visualization and dynamic modulation of the amplified luminescence dissymmetry factor. *J. Mater. Chem. C* **10**, 7311–7318 (2022).
41. Feng, Z. et al. Dynamic multimodal information encryption combining programmable structural coloration and switchable circularly polarized luminescence. *Nat. Commun.* **16**, 2264 (2025).
42. Wen, L. et al. Multi-responsive circularly polarized luminescence micro-patterns with high Fig. of merit towards multi-dimensional data encoding. *Chem. Eng. J.* **505**, 159821 (2025).
43. Xie, Y. et al. Inverse design of chiral functional films by a robotic AI-guided system. *Nat. Commun.* **14**, 6177 (2023).
44. Lin, S. et al. Photo-triggered full-color circularly polarized luminescence based on photonic capsules for multilevel information encryption. *Nat. Commun.* **14**, 3005 (2023).
45. Li, L.-Y., Tan, Q.-W., Wang, X.-L., Wang, Y.-Z. & Song, F. Bioinspired hierarchical photonic structures with controllable polarization and color for optical-multiplexed information encryption. *ACS Nano* **19**, 6426–6436 (2025).
46. Xu, M. et al. Designing hybrid chiral photonic films with circularly polarized room-temperature phosphorescence. *ACS Nano* **14**, 11130–11139 (2020).

Acknowledgements

This study was supported by the National Natural Science Foundation of China (No. 52373122, G.Z.), the Young Scientist Fund of the National Natural Science Foundation of China (No. 52403119, Y.X.; No. 52503119, H.Z.). Fundamental Research Funds for the Central Universities (No. WK2060000078, Y.X.). Youth Project of the Provincial Natural Science Foundation of Anhui (No. 2408085QB041, H.Z.), the open research fund of Suzhou Laboratory (No. SZLAB-1508-2024-ZD017, H.Z.), Double First-Class Initiative University of Science and Technology of China (No. KY2400000037, J.L.), the Young Talent Programme (No. GG2400007009, J.L.), and AnHui Estone Materials Technology Co., Ltd. This work was partially carried out at the University of Science and Technology of China's Center for Micro and Nanoscale Research and Fabrication, and the Instruments Center for Physical Science. Thanks to Prof. Jun Jiang and Dr. Jiahui Du for their support of the theoretical simulation. The AI-driven experiments, simulations, and model training were performed on the robotic AI-Scientist platform of the Chinese Academy of Sciences. This work was supported by USTC Bihe Youth Program for Interdisciplinary Innovation (No. BH-202506, X.C.).

Author contributions

G.Z., F.W., Y.X., and H.Z. were responsible for the overall project design, direction, and supervision. X.C. conducted the synthesis and characterization of all samples and wrote the paper. D.W. and L.G. performed the CD measurements and analysis. X.L., P.Y., and Z.F. contributed to the preparation of $Cu(OH)_2$ nanowires. J.L. contributed to g_{lum} measurements and analysis. All authors contributed to the discussion of results and paper writing.

Competing interests

The authors declare no competing interests.

Additional information

Supplementary information The online version contains supplementary material available at https://doi.org/10.1038/s41467-025-65310-0.

Correspondence and requests for materials should be addressed to Hongli Zhang, Yifan Xie, Fei Wang or Gang Zou.

Peer review information *Nature Communications* thanks Xiao-Ping Zhou and the other, anonymous, reviewer(s) for their contribution to the peer review of this work. A peer review file is available.